Journal Pre-proof

Experimental investigation of NO reduction by H_2 on Pd using planar laser-induced fluorescence

Sui Wan, Thomas Häber, Patrick Lott, Rainer Suntz, Olaf Deutschmann

PII: S2666-352X(23)00118-8
DOI: https://doi.org/10.1016/j.jaecs.2023.100229
Reference: JAECS 100229

To appear in: *Applications in Energy and Combustion Science*

Received date : 31 August 2023
Revised date : 21 October 2023
Accepted date : 18 November 2023

Please cite this article as: S. Wan, T. Häber, P. Lott et al., Experimental investigation of NO reduction by H_2 on Pd using planar laser-induced fluorescence. *Applications in Energy and Combustion Science* (2023), doi: https://doi.org/10.1016/j.jaecs.2023.100229.

Available online at www.sciencedirect.com

ScienceDirect

Applications in Energy and Combustion Science 00 (2023) 1–14

Experimental investigation of NO reduction by H_2 on Pd using planar laser-induced fluorescence

Sui Wan[a], Thomas Häber[a], Patrick Lott[b], Rainer Suntz[b], Olaf Deutschmann[a,b,*]

[a]*Institute of Catalysis Research and Technology (IKFT), Karlsruhe Institute of Technology (KIT), Eggenstein-Leopoldshafen 76344, Germany*
[b]*Institute for Chemical Technology and Polymer Chemistry (ITCP), Karlsruhe Institute of Technology (KIT), Karlsruhe 76131, Germany*

Abstract

This study investigates the NO reduction by H_2 on a Pd/Al_2O_3 catalyst in a temperature range of 100 − 300 °C and NO/H_2 ratios from 0.5 − 2, aiming to gain a deeper understanding of the reaction kinetics and its interaction with mass transfer. Planar laser-induced fluorescence (PLIF) is used to visualize the NO distributions over the catalyst, supplemented by end-of-pipe gas analysis of other components. The reduced Pd-based catalyst undergoes a slow deactivation after exposure to the reactive flow, leading to reduced overall NO conversion and decreased selectivity towards N_2. The NO-PLIF measurements are only conducted on the reduced catalyst without considering the temporal evolutions. Despite the overall NO conversion varying only around 50-65% across all the investigated conditions, the spatially resolved NO distributions reveal three distinct regimes that limit the overall NO conversion: the regime governed by intrinsic reaction rates, the regime constrained by H_2 availability, and the regime restricted by NO diffusion. These findings, demonstrating the interaction between reaction kinetics and mass transfer over a heterogeneous catalyst, highlight the significance of analyzing spatially resolved concentration distributions obtained through PLIF measurements. This approach complements the conventional end-of-pipe analysis, offering a more comprehensive understanding of the underlying processes.

Keywords: NO reduction by H_2, Pd/Al_2O_3, Planar laser-induced fluorescence (PLIF), Spatial distribution, Diffusion limitation

1. Introduction

In recent years, good progress has been achieved in reducing CO_2 emissions by promoting renewable energies, setting emission targets, and implementing policies toward carbon neutrality. Hydrogen-based renewable energy technologies, such as hydrogen combustion and hydrogen fuel cells, are being widely recognized as crucial means to attain a sustainable and zero-carbon future [1–4]. However, when H_2 reacts with O_2 in the presence of N-containing compounds, such as during H_2 combustion with air, NOx emissions may occur due to high reaction/combustion temperatures [5–7]. (Ultra-)lean combustion has been proposed to suppress NOx emissions, however, this comes at the expense of thermal efficiency [8]. As a result, there is a growing demand for efficient and environmentally friendly NOx removal technologies [9]. The selective catalytic reduction of NOx with H_2 is considered as one of the most promising options, since H_2 is usually available both as a fuel and as a reductant and because H_2O is the only product from the H_2-O_2 reaction [10–12].

*Corresponding author
Email address: deutschmann@kit.edu (Olaf Deutschmann)

H_2-SCR, which typically takes place over catalysts with platinum group metals (PGMs) as the active component, has been extensively studied [13–16]. The reaction occurs through multiple pathways:

$$2\,NO + 5\,H_2 \rightarrow 2\,NH_3 + 2\,H_2O \quad \text{(R1)}$$

$$2\,NO + 2\,H_2 \rightarrow N_2 + 2\,H_2O \quad \text{(R2)}$$

$$2\,NO + H_2 \rightarrow N_2O + H_2O \quad \text{(R3)}$$

$$2\,NO + O_2 \rightarrow 2\,NO_2 \quad \text{(R4)}$$

$$2\,H_2 + O_2 \rightarrow 2\,H_2O \quad \text{(R5)}$$

Reaction (2) is considered as the most desirable reaction since it converts NO to harmless N_2 and H_2O. However, the formation of other byproducts cannot be entirely avoided. Reactions (1-5) can be divided into two sub-mechanisms. The first sub-mechanism includes Reactions (1-3), which determine the selectivity towards NH_3, N_2, and N_2O. The second sub-mechanism involves combustion reactions (R4-5), primarily contributing to the diminishing reduction efficiency. This is caused either by consuming the reducing agent, H_2, or by oxidizing NO to NO_2, which requires more H_2 for reduction. Generally, Pt-based catalysts exhibit the highest overall activity among all PGMs, particularly at low temperatures ($\leq$ 200 °C) [17]. However, this high activity is often accompanied by high selectivity towards nitrous oxide (N_2O) [15, 16, 18], a greenhouse gas with a 298 times higher global warming potential than CO_2 for a 100-year timescale [19]. Alternatively, Pd-based catalysts are gaining increasing attention due to their higher N_2-selectivity and lower cost compared to Pt-based catalysts [13, 14].

The primary objective of H_2-SCR optimization is to achieve both high NOx conversion and high selectivity towards N_2, which requires a comprehensive understanding of the reaction network. Although experimental results from a wide range of catalyst systems have been reported [13, 14, 20, 21], the gas-phase experimental data from previous literature is often limited to end-of-pipe concentrations. Neglecting the spatial variance along the catalyst bed may lead to a misperceived intrinsic reaction rate, as the overall reaction may be under the mass transfer limitation. Torkashvand et al. demonstrated in their 3D simulation that modeling the final percentages of the unconverted formaldehyde in the catalytic oxidation monolith converter requires considering the local washcoat distributions, rather than solely focusing on elevating the intrinsic reaction rate in the kinetic mechanism [22]. Therefore, spatially resolved concentration data is crucial for accurately assessing the reaction kinetics and mass transport phenomena in H_2-SCR systems.

Gas sampling techniques with capillary probes [23, 24], e.g. SpaciMS and SpaciPro, allow the characterization of 1D concentration or temperature profiles within the catalyst. Moreover, in-situ laser-based techniques have also been applied for catalyst studies, as these are not only non-invasive techniques that are free of bias by possible capillary-induced flow distortion, but commonly offer a higher spatial and temporal resolution. Several pioneering studies with planar laser-induced fluorescence (PLIF) and Raman spectroscopy have been conducted by Mantzaras et al. to investigate catalyst-assisted combustion [25–27]. Zetterberg and Lundgren et al. have utilized PLIF to conduct comprehensive studies on CO oxidation over noble metal catalysts [28–30]. More recently, they have combined PLIF with Raman spectroscopy and near-surface mass spectrometry to acquire detailed gas species distributions during the partial oxidation of methanol [31]. In our previous studies, HCHO-PLIF and NO-PLIF have been used to study the catalytic oxidation of HCHO and NOx storage and removal, respectively [32–36]. Compared with flames, to some extent, heterogeneous catalytic reactions are even more suitable for applying PLIF. This is because compensating for the quenching effect in flames is challenging due to significant variations in species and temperature.

This work investigated the impact of reaction temperature and gas components on the NO reduction by H_2 over a 1 wt.% Pd/Al_2O_3 catalyst-coated plate in a parallel wall channel using NO-PLIF measurements. To achieve a precise understanding of each sub-mechanism, this study excludes the competition between NO and O_2 for H_2, by examining the reaction in the absence of O_2. The focus lies on the selectivity towards the reduction products, NH_3, N_2, and N_2O. Furthermore, by visualizing the local NO concentration distributions, the interaction between the surface reaction kinetics and mass transport is discussed in detail. Three distinct regimes that constrained the overall NO conversion have been uncovered, demonstrating the significance of spatially resolved data, particularly for catalytic systems involving multiple reaction pathways.

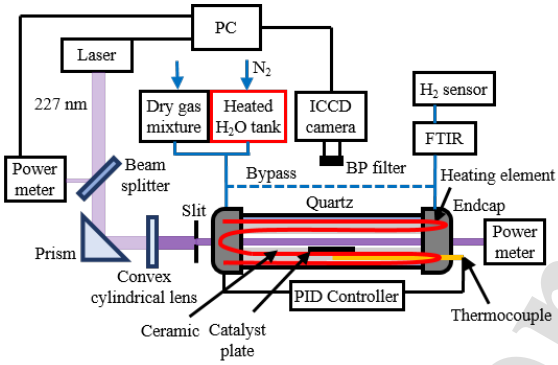

Figure 1. Schematic of the experimental setup for NO-PLIF measurements with controlled dosing of H_2O vapor in the gas mixture.

2. Experimental Methods

2.1. Catalyst materials

Analogous to one of our previous studies [35], the catalyst was prepared via incipient wetness impregnation (IWI). For this, the catalyst support, γ-Al_2O_3 (Puralox, SASOL Germany GmbH), was first calcined at 700 °C for 5 hours. Palladium (Pd) was then introduced using an aqueous tetraamminepalladium(II)nitrate solution (abcr, 5.0 wt.% Pd) as a precursor, targeting a 1 wt.% Pd/Al_2O_3 catalyst powder sample. The received powder was dried at 70 °C for 2 hours and subsequently calcined at 550 °C for 5 hours in static air. The catalyst powder and AlO(OH) (Disperal P2, SASOL) are mixed in a weight-ratio of 9 to 1 and water is added to form an aqueous slurry. The amount of the slurry, containing approximately 50 mg of Pd/Al_2O_3 catalyst powder, was applied to the upper surface of an 18 mm wide, 25 mm long, 1 mm thick section of a monolithic cordierite substrate (NGK, 3.0 mil, 600 cpsi) by using a syringe. Careful rotation and tilting of the substrate ensured a uniform distribution of the slurry. After drying in a static air environment, the coated plate was subjected to a further calcination at 600 °C for 5 hours in static air to ensure secure adhesion of the washcoat onto the cordierite substrate.

The specific surface area and the total pore volume of the powder catalyst was assessed by N_2-physisorption using a Belsorp mini II (MicrotracBEL) and subsequent evaluation according to the BET method. The BET surface area of the Pd/Al_2O_3 powder is 173 m^2/g, and the total pore volume is 0.48 mL/g. The noble metal dispersion, determined through a CO chemisorption measurement, is 43%.

2.2. NO-PLIF over catalyst-coated plate

The experimental setup for the NO-PLIF measurements over a 1 wt.% Pd/Al_2O_3 catalyst-coated plate is illustrated in Fig. 1, which is similar to that described in our previous studies [32–36]. 0.5 mg Pd/Al_2O_3 catalytic powder is coated on the top surface of an 18 mm wide, 25 mm long plate, which is placed in a ceramic holder to form a 2 mm high parallel wall channel in a quartz pipe. The channel is sealed, and a uniform temperature field is achieved by the heating control unit. The gases are introduced into the reactor using mass flow controllers (MFCs) in combination with 3/2-way solenoid valves, which allow for the control of flow directions - either into the reactor or bypassing it. A heated water tank is connected into the gas line, allowing water vapor to be carried along when N_2 flows through. By controlling the heating temperature and the mass flow of the N_2 carrier gas, the concentration of H_2O in the inlet gas mixture can be accurately regulated.

After placing the sample in the reactor, the calcined catalyst-coated plate undergoes an additional in-situ oxidation at 450 °C for 12 hours with a 10% O_2 in N_2 gas flow. This step eliminates any potential contamination that might have occurred during the reactor assembly process. After purging with inert gas, the sample is then reduced by 10% H_2 in N_2 at 400 °C for 2 hours. A final purging with inert gas is then performed to ensure that no H_2 remains in the system.

All experiments are conducted at atmospheric pressure with a total flow rate of 1 L/min (NTP ≡ 1 atm & 20 °C). Considering the dimensions of the parallel wall channel and the given flow rate, the experimental conditions are comparable to those of a 100 cpsi monolith catalyst operating with a gas hourly space velocity of 60000 h^{-1}. A de- and reactivation test is performed to ensure that all PLIF measurements are carried out with the catalyst in the same status. The influences of temperature (ranging from 100 to 300 °C) and inlet H_2 concentration (varying from 200 to 800 ppm) are investigated in this study, with a fixed NO concentration of 400 ppm and H_2O concentration of 1%, balanced with N_2. In this study, H_2O in the feed gas has been used as the dominant quencher to mitigate the effects of spatially non-uniform fluorescence quenching. Further details are provided in the next section. Selecting H_2O as the dominant quencher and N_2 as the carrier gas, rather than other combinations of gases, such as CO_2 and Ar that are chemically fairly inert under the conditions applied throughout this study [37] but do not belong to the products, limits the ability to directly measure H_2O and N_2 formation. Nevertheless, their formation can still be accurately calculated through mass balance. This choice closely aligns with real-world conditions in industrial applications, particularly in the rapidly advancing field of H_2-based renewable energy technologies.

The detection of NO is accomplished by exciting the $P_2(12.5) + Q_{12}(12.5)$ line in the NO $A^2\Sigma^+ \rightarrow X^2\Pi$ (0,0) band with a UV laser at 226.67 nm [32], and collecting fluorescence through an image-intensified charge-coupled device (ICCD) camera (IRO 25 & Imager QE, LaVision) with a band pass-filter centred at 248 nm (FWHM = 10 nm, peak transmission 15%, LaVision). The 10 Hz excitation laser is generated by a frequency-doubled Nd:YAG (Quanta-Ray Pro, Spectra-Physics) pumped dye laser (PrecisionScan, Sirah) sum-frequency mixed with the third harmonic output of the same Nd:YAG laser. A Fourier-transform infrared spectrometer (FTIR) (MG2030, MKS) and a mass spectrometer (MS) optimized for H_2 quantification (HSense, MS4) are connected to the exhaust of the reactor to monitor the NO, N_2O, NH_3, H_2O and H_2 concentrations at the outlet and can be alternatively switched to the bypass connection for measuring the inlet concentrations.

2.3. Calibration of PLIF signal

All measurements are conducted with the laser power in the linear LIF regime. The fluorescence intensity is given by Equation (1) [38],

$$F = C_{exp} B_{12} I_v N_{NO} f_1 \frac{A_{21}}{A_{21} + Q_{21}} \tag{1}$$

where C_{exp} is an experimentally derived constant, B_{12} is the Einstein coefficient for photon absorption, I_v is the local laser energy, N_{NO} is the number density of NO molecules, f_1 is the Boltzmann factor, A_{21} is the spontaneous emission coefficient and Q_{21} is the collisional quenching rate. Therefore, the local absolute NO concentration under reactive conditions, C_{NO}, can be calculated by comparing the PLIF image of the reactive flow to a reference image captured under non-reactive conditions in the same system at an identical temperature. Disregarding minor differences in the laser absorption by NO above the catalytic plate, the local laser intensity distributions for both the target and reference images can be considered as identical. Therefore, the ratio of the local laser energy (I_v) between the two images is equivalent to the ratio of the total laser beam energy (I_{beam}) employed during the acquisition of these images. The local NO concentration under reactive conditions is given by Equation (2).

$$C_{NO} = C_{NO,ref} \frac{I_{beam,ref}}{I_{beam}} \frac{F}{F_{ref}} \frac{A_{21} + Q_{21}}{A_{21} + Q_{21,ref}} \tag{2}$$

Herein, the subscript ref stands for the values under the reference condition. $C_{NO,ref}$ is determined by the setting of MFCs and additionally monitored by the FTIR. I_{beam} and F are the measured values. The determination of the total collisional quenching rate, Q_{21}, requires the information on the local concentration for each gas component according to Equation (3).

$$Q_{21} = \Sigma \sigma_{Qi} \langle v_i \rangle N_i \tag{3}$$

σ_{Qi} is the cross section for collisional quenching of NO $A^2\Sigma^+(v' = 0)$ by species i, $\langle v_i \rangle$ is the average collision velocity of the collision pair, NO and species i, and N_i is the number density of species i. However, obtaining the local gas concentrations with NO-PLIF solely is not feasible due to the unknown local selectivity among the multiple reaction pathways. Thus, similar to our previous studies, a dominant quencher, H_2O for this study, has been added into the flow to keep the total collisional quenching rate approximately uniform in the entire channel. Paul et al. reported

comprehensively on the quenching of NO $A^2\Sigma^+$ based on a wide range of experimental data, and developed models that provide physically plausible fits to the measurements [38–40]. The predicted quenching cross sections for NO fluorescence are summarized in Table 1.

Table 1. Cross sections for collisional quenching of NO $A^2\Sigma^+$ ($v' = 0$) calculated from the model by Paul et al. [40].

Species	σ_Q [Å^2] at 100 °C	σ_Q [Å^2] at 300 °C
NO	43.0	43.0
NH_3	97.5	81.2
N_2	0.019	0.072
N_2O	79.5	70.8
H_2	≈ 0	≈ 0
H_2O	87.5	48.5

Considering that only σ_Q for H_2O exhibits a significant decrease from 100 to 300 °C, and NH_3 exhibits the largest σ_Q among the products from NO, the maximum error caused by the non-uniform local quenching effect in this study can be estimated by assuming a 400 ppm NH_3 local production at 300 °C. In this worst-case scenario, the value of the last term in Equation (2), $\frac{A_{21} + Q_{21}}{A_{21} + Q_{21,ref}}$, amounts to 1.032. This implies that when computing the local NO concentration using Equation (4) without accounting for the non-uniform local quenching effect, the calculated local NO concentration can have a maximum discrepancy of 3.2% compared to the actual value.

$$C_{NO} = C_{NO,ref} \frac{I_{beam,ref}}{I_{beam}} \frac{F}{F_{ref}} \tag{4}$$

3. Results and discussion

3.1. Catalyst deactivation experiment

In Fig. 2, the FTIR-measured outlet concentrations of NO, NH_3, and N_2O, along with the calculated N_2 formation, are plotted for the aging test conducted at 300 °C. The inlet gas mixture used for this test consists of 400 ppm NO,

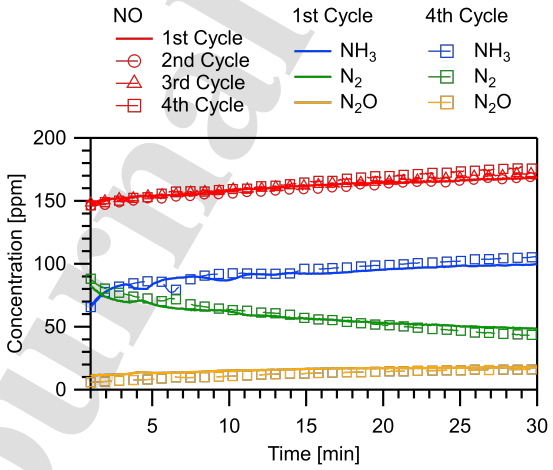

Figure 2. Time-dependent FTIR-measured outlet concentrations for four repeated de- and reactivation cycles of Pd/Al_2O_3 catalyst. N_2 formations are calcluated from mass balance. Inlet: 400 ppm NO, 400 ppm H_2, 1% H_2O, balanced with N_2, T = 300 °C.

400 ppm H_2, 1% H_2O, and balance N_2. The first cycle starts immediately after the pretreatment. As time progresses, a gradual decrease in NO conversion is observed. However, the products NH_3 and N_2O exhibit an increasing yield over time. The decreased NO conversion is attributed to the reduced N_2 formation. Between t = 1 min and t = 30 min, despite only a slight decrease in NO conversion from 63% to 60%, the selectivity to N_2 significantly dropped from 65% to 42%. A deactivation test was also conducted at a lower temperature (T = 100 °C) (data not shown). Compared to the higher temperature, the aging effect at lower temperature was found to be much less pronounced. The gradual decline in performance is likely attributed to the evolution of structure and chemical state of Pd nanoparticles during the reaction. The redispersion of metallic Pd on the support and the subsequent formation of species, including Palladium ion (Pd^{2+}), partially oxidized Palladium ($Pd^{\delta+}$), and Palladium oxide (PdO), have been reported in previous studies, as a result of the reduced catalyst being exposed to reactive flows [41–43].

In contrast to the reversible deactivation observed during NO reduction by CO on Pt-based catalysts, where the catalyst can be reactivated by flowing inert gas [44], the aging effect on the Pd-based catalyst can only be reversed through a reduction process with H_2. Such observation provides support to the notion that the performance drop of the Pd catalyst is linked to the transition from a metallic state to an oxidized state. Previous studies have also reported that the reduction of oxidized Palladium by H_2 can efficiently occur at temperatures as low as 100 °C [45, 46]. A total of four cycles were performed at T = 300 °C. Between each cycle, the catalyst plate was reduced with 400 ppm H_2 in N_2 for 30 minutes, followed by purging with N_2 until H_2 was not detectable. Notably, a high level of reproducibility was observed between each cycle, as shown in Fig. 2. Consequently, instead of performing a complete pretreatment involving both oxidation and reduction pripor to each subsequent measurement conducted under different conditions, the catalyst was only subjected to a 30-minute reduction process with 400 ppm H_2 in N_2, followed by purging with N_2. Furthermore, considering the mild changes in NO conversion over an extended period, this study does not explore the temporal evolution of the 2D NO distributions. All NO-PLIF measurements were consistently conducted at t = 5 min with an average of 300 consecutive laser shots (data acquisition time = 30 s, according to 10 Hz repetition rate). Therefore, the catalyst plate has only been exposed to the reactive flow for less than 6 minutes before undergoing the shortened reduction process.

3.2. Catalytic activity measurement

To evaluate the impact of temperature and inlet gas composition on the catalytic activity and the product selectivity, NO-PLIF measurements, along with end-of-pipe analysis of the effluent gas stream, are performed in the channel reactor over the 1 wt.% Pd/Al_2O_3 catalyst-coated plate. As previously mentioned, all data are collected 5 minutes after the reactive flow is initiated. The data acquisition time is only 30 seconds, which is significantly shorter than the time scale of the aging process. As a result, no temporal evolution is considered in the following data analysis.

Figure 3 illustrates the impact of temperature on the conversions and product yields based on the end-of-pipe measurements at the reactor outlet. The inlet gas mixture consists of 400 ppm NO, 400 ppm H_2, 1% H_2O, and balance N_2. When the temperature is increased from 100 to 200 °C, the NO conversion remains approximately 50%; however, the H_2 conversion rises significantly from 42% to 96%. Within this temperature range, the N_2 formation remains consistently around 20 ppm. Nevertheless, there is a remarkable increase in NH_3 formation with the increased temperature, along with a corresponding decrease in N_2O formation, particularly noticeable in the temperature range of 100 to 150 °C. Between 200 and 300 °C, nearly full conversion of H_2 is achieved in the channel reactor, indicating that H_2 diffusion is not the limiting factor for its consumption under these conditions, likely due to the large diffusion coefficient of H_2, which is approximately 4 times larger than that of NO. In the meantime, NO conversion gradually increase from 49% to 62%, accompanied by an increased N_2 production from 25 to 61 ppm. Figure 3(b) displays the contribution of each competing reaction pathway (R1-3) to the overall NO conversion, which is referred to as the NO reaction path share. It is important to note that the formation of one NH_3 molecule requires one NO molecule (R1), whereas the formation of one N_2 or one N_2O molecule needs two NO molecules (R2, R3). As a result, at T = 300 °C, despite the higher NH_3 concentration at the outlet, only 43% of NO consumption result in NH_3 formation, whereas 49% of NO consumption account for N_2 formation. In the temperature range of 100 to 300 °C, it is observed that only the NO reaction path share for N_2 formation (R2) is monotonically increasing. Considering the stoichiometric coefficients of H_2 in the chemical equations (R1-3), it becomes evident that the apparent reaction rate of NH_3 formation (R3) should be enhanced by an excess of H_2, which is in contrast to the formation of N_2O (R1). However, at T = 100 °C, although more than half of the H_2 remains after passing through the reactor, over 70% of NO are consumed for the formation of N_2O. On the other hand, at $T \geq$ 150 °C, the NO reaction path share for N_2O formation (R3) remains

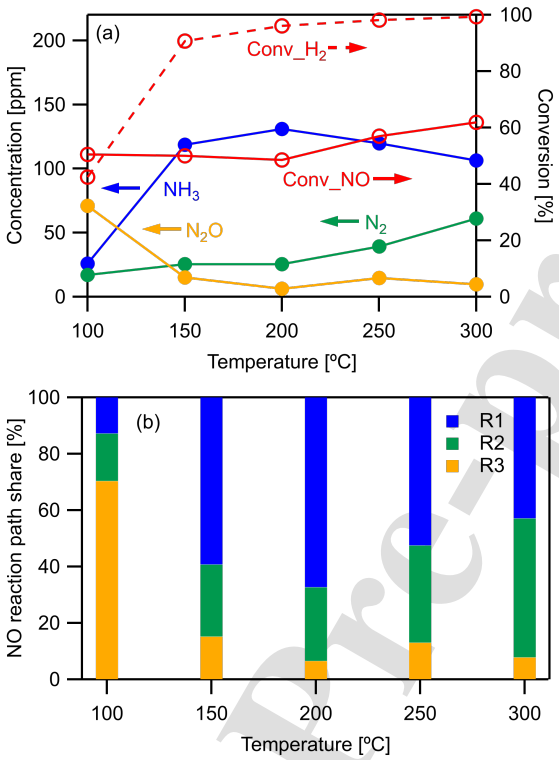

Figure 3. Results with an inlet gas mixture of 400 ppm NO, 400 ppm H_2, 1% H_2O, balanced with N_2 in the temperature range of 100 - 300 °C. (a) Formation of the reaction products and conversion of the reactants. (b) Reaction shares of different NO reaction pathways. R1: Formation of NH_3, R2: Formation of N_2, R3: Formation of N_2O.

less than 15%, irrespective of the low H_2 concentration at outlet. The results indicate that the formation of N_2O is much more favored at lower temperatures, while the low temperatures inhibit the formation of NH_3. Similar changes in selectivity with varying temperatures have been reported in other literature [17, 21]. The NO reaction path share for NH_3 formation (R1) decreases from 67% at 200 °C to 43% at 300 °C. The inhibited NH_3 formation at higher temperature is likely due to the more favored N_2 formation under the conditions with a limited amount of H_2.

The impact of the inlet H_2 concentration on the catalyst performance has been investigated at T = 300 °C, and the results are shown in Fig. 4. As expected from the stoichiometric relation, the formation of NH_3 significantly increases with the higher H_2 concentration at the inlet. Meanwhile, the NO reaction path share for N_2O formation (R3) decreases from 24% with 200 ppm H_2 at the inlet to 0% with 800 ppm H_2 at the inlet. However, even though the coefficient ratio between NO and H_2 is 2 for N_2O formation (R3) and 1 for N_2 formation (R2), with 400 ppm NO and 200 ppm H_2 at the inlet, the formation of N_2 remains the dominant reaction path. Besides the reaction kinetic reasons, the much slower diffusion of NO compared to H_2 also contributes to a reduced local NO/H_2 ratio over the catalyst plate. The stoichiometric coefficient ratio between NO and H_2 is 0.4 for NH_3 formation (R1). According to this stoichiometric relation, it is theoretically possible to achieve full conversion of H_2 with a gas mixture consisting of 400 ppm NO and 800 ppm H_2. However, when the inlet H_2 concentration is raised to 800 ppm, the H_2 conversion reduces from full conversion to 72%. This reduction is partially attributed to the limited diffusion rate of NO, which will be further discussed in the later analysis of the NO spatial distribution.

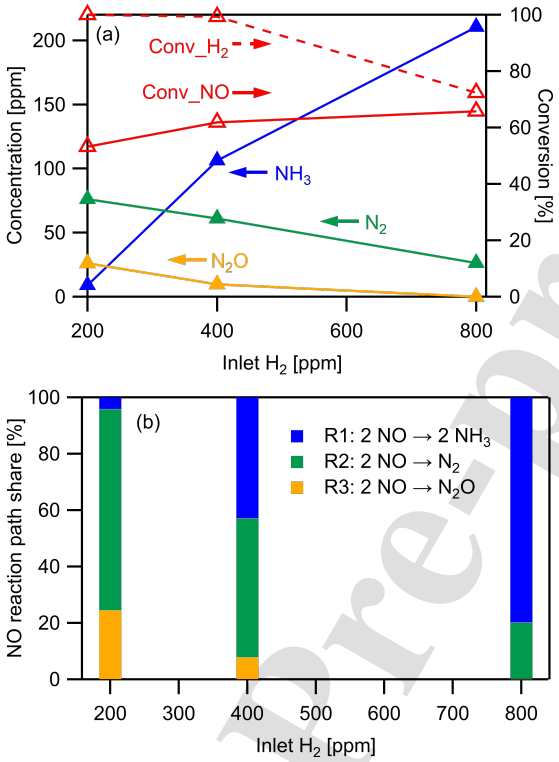

Figure 4. Results at T = 300 °C with an inlet gas mixture of 400 ppm NO, 200 - 800 ppm H_2, 1% H_2O, balanced with N_2. (a) Formation of the reaction products and conversion of the reactants. (b) Reaction shares of different NO reaction pathways. R1: Formation of NH_3, R2: Formation of N_2, R3: Formation of N_2O.

3.3. *Spatially resolved NO distribution over catalyst plate*

Figure 5 shows the NO-PLIF images acquired over the 1 wt.% Pd/Al_2O_3 catalyst-coated plate in the 2 mm high channel under selected conditions. The position of the sample plate is marked as the pink line at the bottom of each sub-figure. The spatial resolution of the PLIF images is 22 µm/pixel. Uniform NO distribution is observed before the catalyst plate, indicating that no gas-phase reaction happens under the given conditions, and the streamwise diffusion is not significant. Under the influence of surface reactions, diffusive and convective mass transfer, NO concentration gradients appear in both wall-normal and streamwise directions above the catalyst plate. The concentration gradients vary at distinct locations and also under different conditions. For a better comparison of quantities, the NO concentration profiles extracted from Fig. 5 are plotted in Fig. 6 and 7. The profiles in the streamwise direction represent averaged NO concentrations over the entire channel height, while the profiles in the wall-normal direction show the local NO concentration distributions at x = 5 mm (dashed lines) and 20 mm (solid lines). The local net NO consumption rate can be evaluated from these spatially resolved profiles using the following two approaches: (1) By dividing the channel into small finite elements in the streamwise direction, the local net NO consumption rate is determined by the mass difference between the NO flowing into and out of each small finite element. Since the mass flow rate is constant for all conditions, regardless of thermal expansion due to variations in reaction temperature, the gradient of the averaged NO concentration in streamwise direction directly reflects the local NO mass loss. It is to note that, within this discussion, the term ”concentration” refers to the mole fraction in units of ppm, rather than the molar concentration expressed in mol/L. (2) Considering that the flow velocity at the wall boundaries is zero, the conductive

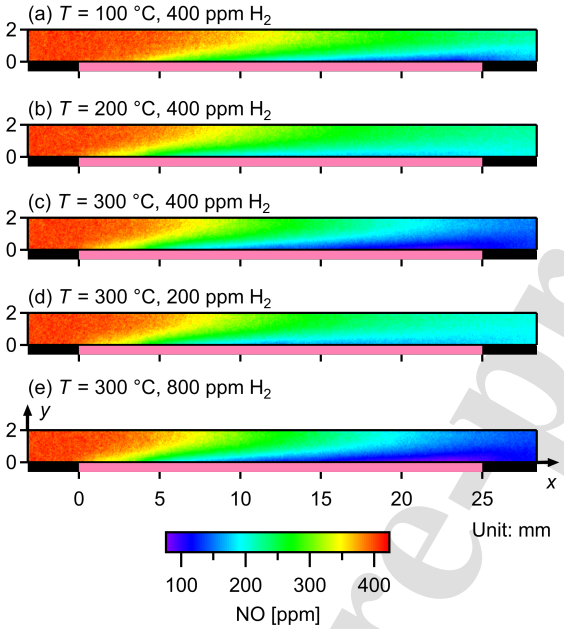

Figure 5. PLIF-measured NO distributions over the 1 wt.% Pd/Al_2O_3 catalyst-coated plate (marked as the pink line) in the 2 mm high parallel wall channel.

mass transfer in the vicinity of the catalytic surface becomes negligible. Therefore, the local net NO consumption rate can reasonably be approximated as equal to the NO mass flux driven by diffusive mass transfer near the catalytic surface, which can be evaluated by the local NO concentration gradient in the wall-normal direction. However, it should be noted that the differences in gas density and diffusion coefficient stemming from temperature variations should be taken into consideration when comparing cases with different temperatures. In addition to the local NO consumption rate, the NO concentration profiles in the wall-normal direction provide valuable information for assessing diffusive mass transfer.

When comparing T = 100 and 200 °C, the NO concentrations at the outlet are approximately at the same level. However, as depicted in Fig. 6 (a), at T = 100 °C, the NO conversion along the catalyst plate shows minor variation, whereas at T = 200 °C, a much faster NO conversion is observed upstream, but a slower one downstream. This pattern is also evident in the wall-normal concentration gradients, where at x = 5 mm (dashed lines), a much larger concentration gradient is observed at T = 200 °C, while at x = 20 mm (solid lines), the concentration gradient at T = 100 °C becomes more pronounced. The observed results can be related to the difference in the overall H_2 conversion as shown in Fig. 3 (a). At lower temperature (T = 100 °C), the formation of N_2O, which consumes much less H_2, is favored over NH_3 formation. Consequently, 58% of H_2 from the feed gas remain after flowing through the reactor, indicating the availability of H_2 for reacting with NO downstream. At upstream, subtle concentration gradients of NO are observed both in the streamwise and wall-normal directions, indicating a relatively low local NO conversion rate. In the vicinity of the catalyst surface, the relatively high local NO concentration at x = 5 mm implys that NO mass transfer does not predominantly restrain the NO conversion rate here. Considering the availability of H_2 and the significantly faster diffusion of H_2 in comparison to NO, the primary constraint on the local NO conversion rate is rooted in the intrinsic reaction rates. A gradual decrease in the concentration gradient of reactants is typically anticipated along the streamwise direction. This expectation arises from the diminishing rate of reactant consumption correlated with the declining reactant concentrations. However, a slight anomaly emerges

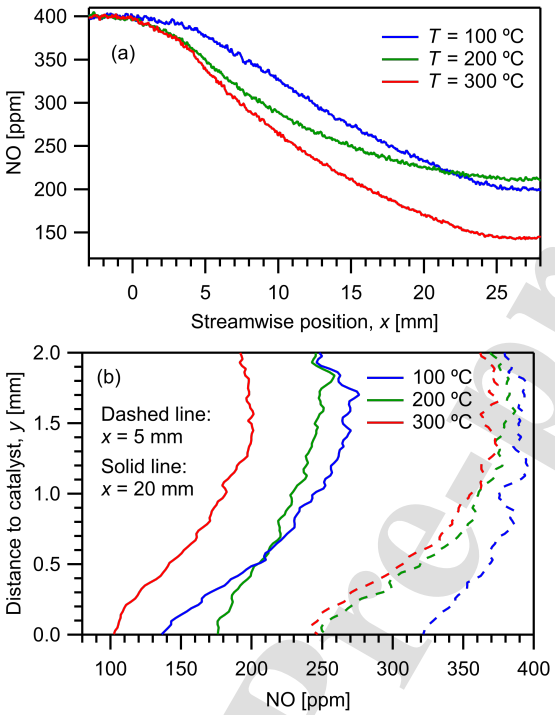

Figure 6. NO concentration profiles extracted from PLIF images captured in the temperature range of 100 - 300 °C with an inlet gas mixture of 400 ppm NO, 400 ppm H_2, 1% H_2O, balanced with N_2. (a) Streamwise direction averaged over the channel height. (b) Wall normal direction.

at T = 100 °C, where minor concentration gradient variation has been observed. Notably, despite the remarkably lower local NO concentration near the surface at x = 20 mm, a minor elevation in the NO concentration gradient in the wall-normal direction is even observed in comparison to the situation at x = 5 mm. These observations suggest the selectivity variations throughout the catalyst bed. A more effective pathway for NO consumption is enhanced downstream, possibly attributed to the changes in the local NO/H_2 ratio. In contrast to the scenario at T = 100 °C, the observed sharp NO concentration gradient upstream at T = 200 °C signifies an accelerated net NO consumption rate. This rise in the net NO consumption rate, even with a reduced gas number density resulting from the elevated temperature, serves as a distinct indication of the pronounced temperature-dependent increase in intrinsic reaction rates. Moreover, in the upstream region, the notable NO concentration gradient in the wall-normal direction provides clear evidence that the local NO consumption rate in this area is strongly influenced by NO diffusion. However, downstream, the diminished NO concentration gradients imply a lessened limitation due to NO diffusion. On the other hand, at T = 200 °C, the H_2 conversion increases to 96% as the NO reaction path share for NH_3 formation reaches its maximum, as shown in Fig. 3. It is very likely that the major H_2 consumption has already occurred upstream by forming NH_3, leading to a significantly reduced NO conversion rate downstream due to the lack of H_2.

As the reaction temperature raised from 200 to 300 °C, an enhanced NO conversion is observed downstream, despite the further increase in H_2 conversion. This enhancement can be attributed to the higher selectivity towards N_2 formation at the elevated temperature. Since the formation of N_2 (R2) consumes less H_2 compared to NH_3 formation (R1), a larger amount of H_2 remains available for reaction downstream, thereby maintaining the NO conversion rate along the entire channel. As shown in Fig. 6 (b), the NO concentration gradients at T = 200 and 300 °C are similar at both x = 5 and 20 mm. Considering that the diffusion coefficient is proportional to $T^{1.5}$ and gas density is proportional

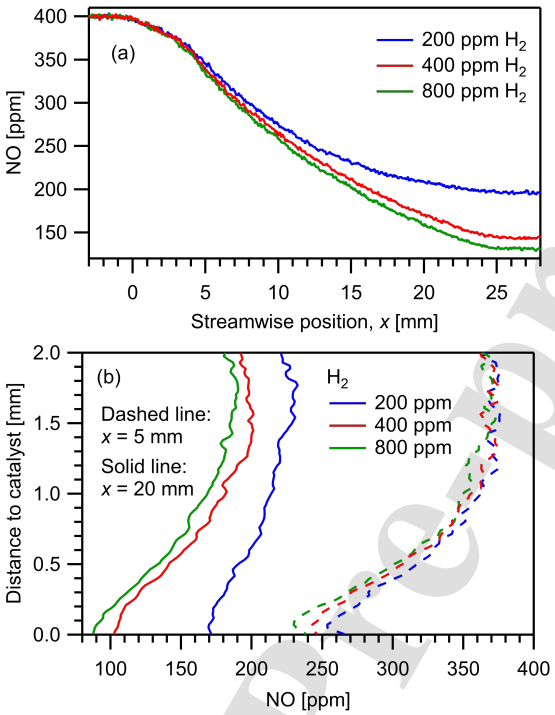

Figure 7. NO concentration profiles extracted from PLIF images captured at 300 °C with an inlet gas mixture of 400 ppm NO, 200 - 800 ppm H_2, 1% H_2O, balanced with N_2. (a) Streamwise direction averaged over the channel height. (b) Wall normal direction.

to T^{-1}, a faster diffusion-driven NO mass flux at the catalytic surface can be expected at the higher temperature, when such wall-normal concentration gradients remain similar. Evidently, the local net NO consumption rate, which is approximately equal to this diffusion-driven mass flux, is expected to be higher along the entire channel at T = 300 °C. This faster conversion is attributed not only to the higher intrinsic reaction rate but also to the selectivity shift towards the more efficient NO consuming reaction pathway (from R1 to R2).

Figure 7 compares the NO concentration profiles at T = 300 °C with varying inlet H_2 concentrations. As shown in Fig. 4, a full conversion of H_2 is reached with either 200 ppm or 400 ppm H_2 at the inlet. NO concentration gradients at x = 5 mm are very similar under these two conditions; however, with less H_2 in the feed gas, the NO conversion downstream is greatly suppressed. The significant reduction in the downstream NO concentration gradients bear resemblance to the situation depicted in Fig. 5 (b), with 400 ppm H_2 at T = 200 °C. In both cases, the overall NO conversion is constrained by the availability of H_2 downstream. When the inlet H_2 concentration increases from 400 to 800 ppm, the H_2 conversion reduces, indicating that more H_2 is available to react, especially at downstream position. Nevertheless, the NO distributions in both streamwise and wall-normal directions maintain a similar shape along the entire channel. The fact that the NO conversion rate remains unchanged despite having more potential reacting partners suggests that the NO conversion under these conditions is limited by the NO diffusive mass transfer. The diminished NO concentration in the vicinity of the catalytic surface further supports this proposition. However, with a larger amount of H_2 feeding, the local H_2 concentration becomes much higher, resulting in a significant increase in selectivity towards NH_3 formation.

The local gas concentration distributions play a crucial role in heterogeneous catalytic reactions, particularly when multiple reaction pathways are involved. At low reaction temperatures, e.g. T = 100 °C, the NO conversion is primar-

ily limited by the low intrinsic reaction rate, particularly in the reaction path of NH_3 formation. Consequently, both NO and H_2 undergo limited overall conversions. However, the concentration gradients in the wall-normal direction indicate that the overall reaction rate is still affected by diffusion. At elevated temperatures with a limited quantity of H_2 in the feed gas, remarkable variations in NO concentration gradients are observed between the upstream and downstream regions. This observation suggests that NO conversion is predominantly consumed upstream, and the reaction progression is impeded downstream due to the lack of H_2. Importantly, this phenomenon is not only observed under conditions with a NO/H_2 ratio greater than 1, it is also applicable under conditions favoring NH_3 formation, which leads to rapid upstream H_2 consumption. A NO diffusion-limited regime emerges at elevated temperatures with a low NO/H_2 ratio. Despite an excess of H_2 and the elevated intrinsic reaction rates, the overall conversions of both NO and H_2 are hindered by the diffusion rate of NO. For all cases, due to the significant difference in the diffusion coefficients between NO and H_2 molecules, the local NO/H_2 ratio at the catalytic surface tends to be higher than the averaged NO/H_2 ratio on the cross-sections. This leads to a selectivity towards those reaction paths that are favored by higher concentrations of H_2. Quantitative comparisons of the chemical reaction timescales, diffusive and convective mass transfer timescales, using dimensionless numbers such as the Damköhler number, would offer a clearer understanding of how the controlling factors shift among all conditions [47]. Future numerical and experimental investigations will continue to enhance this discussion after revealing local H_2 distributions and the detailed reaction kinetics.

4. Conclusions

Spatially resolved NO concentration distributions were acquired through NO-PLIF measurements conducted over a Pd/Al_2O_3 catalyst plate during the NO reduction by H_2. In combination with end-of-pipe gas analysis, this study has explored the interaction between surface reaction kinetics and mass transfer under diverse temperature and NO/H_2 ratio conditions.

The end-of-pipe gas analysis revealed at lower temperature (T = 100 °C), the formation of N_2O was favored, while NH_3 formation was suppressed. It is also noteworthy that under specific conditions, full H_2 conversion can be achieved, suggesting that the diffusive mass transfer of H_2 is generally not a limiting factor for the overall NO conversion. Spatially resolved NO distributions unveil three distinctive regimes imposing limitations on the overall NO conversion: the regime governed by intrinsic reaction rates, the regime constrained by H_2 availability, and the regime restricted by NO diffusion. The overall conversion, local concentration gradient, and product selectivity are all influenced by the combined effects of kinetics and mass transport. It is essential to highlight that, under distinct reaction conditions, different NO concentration distributions can arise even under a similar overall NO conversion, and differing product selectivities can emerge despite the similarity in shapes of the 2D NO distributions. These findings illustrate the importance of analyzing spatially resolved NO concentration distributions obtained via PLIF measurements, in addition to solely relying on the end-of-pipe analysis. Moreover, considering the envisaged shifts in the local selectivity along the catalyst bed based on diffusion properties, acquiring spatially resolved data for all relevant gas components becomes essential when studying catalytic systems involving multiple reaction pathways. Future investigations will extend to exploring concentration distributions of species beyond NO, contributing to a more comprehensive comprehension of the H_2-SCR system.

Acknowledgement

This work was supported by the Deutsche Forschungsgemeinschaft (DFG, German Research Foundation) via SFB 1441, Project- ID 426888090, and the Helmholtz program “Materials and Technologies for the Energy Transition” (MTET).

References

[1] H. Nazir, N. Muthuswamy, C. Louis, S. Jose, J. Prakash, M. E. Buan, C. Flox, S. Chavan, X. Shi, P. Kauranen, et al., Is the H_2 economy realizable in the foreseeable future? Part III: H_2 usage technologies, applications, and challenges and opportunities, International Journal of Hydrogen Energy 45 (53) (2020) 28217–28239.

[2] S. Zhang, N. Zhang, R. Smith, W. Wang, A zero carbon route to the supply of high-temperature heat through the integration of solid oxide electrolysis cells and H_2-O_2 combustion, Renewable and Sustainable Energy Reviews 167 (2022) 112816.

[3] M. K. Singla, P. Nijhawan, A. S. Oberoi, Hydrogen fuel and fuel cell technology for cleaner future: a review, Environmental Science and Pollution Research 28 (2021) 15607–15626.

[4] P. Lott, U. Wagner, T. Koch, O. Deutschmann, Hydrogen combustion engines–chances and challenges on the way towards a decarbonized mobility, Chemie Ingenieur Technik 94 (3) (2022) 217–229.

[5] Z. Stepień, A comprehensive overview of hydrogen-fueled internal combustion engines: Achievements and future challenges, Energies 14 (20) (2021) 6504.

[6] S. K. Dash, S. Chakraborty, M. Roccotelli, U. K. Sahu, Hydrogen fuel for future mobility: Challenges and future aspects, Sustainability 14 (14) (2022) 8285.

[7] J. Desantes, R. Novella, B. Pla, M. Lopez-Juarez, Impact of fuel cell range extender powertrain design on greenhouse gases and NOx emissions in automotive applications, Applied Energy 302 (2021) 117526.

[8] H. Yamamoto, Investigation on relationship between thermal efficiency and NOx formation in ultra-lean combustion, Tech. rep., SAE Technical Paper (1999).

[9] P. Lott, O. Deutschmann, Heterogeneous chemical reactions - A cornerstone in emission reduction of local pollutants and greenhouse gases, Proceedings of the Combustion Institute 39 (3) (2023) 3183–3215.

[10] H. Hamada, M. Haneda, A review of selective catalytic reduction of nitrogen oxides with hydrogen and carbon monoxide, Applied catalysis A: General 421 (2012) 1–13.

[11] M. Jabłońska, An application of steady-state isotopic-transient kinetic analysis (SSITKA) in DeNOx process, ChemCatChem 13 (3) (2021) 818–827.

[12] P. Forzatti, L. Lietti, I. Nova, E. Tronconi, Diesel NOx aftertreatment catalytic technologies: Analogies in LNT and SCR catalytic chemistry, Catalysis Today 151 (3-4) (2010) 202–211.

[13] M. Borchers, K. Keller, P. Lott, O. Deutschmann, Selective catalytic reduction of NOx with H_2 for cleaning exhausts of hydrogen engines: Impact of H_2O, O_2, and NO/H_2 ratio, Industrial & Engineering Chemistry Research 60 (18) (2021) 6613–6626.

[14] M. Borchers, P. Lott, O. Deutschmann, Selective catalytic reduction with hydrogen for exhaust gas after-treatment of hydrogen combustion engines, Topics in Catalysis (2022) 1–12.

[15] Y. Guan, Y. Liu, Q. Lv, B. Wang, D. Che, Review on the selective catalytic reduction of NOx with H_2 by using novel catalysts, Journal of Environmental Chemical Engineering 9 (6) (2021) 106770.

[16] Z. Liu, J. Li, S. I. Woo, Recent advances in the selective catalytic reduction of NOx by hydrogen in the presence of oxygen, Energy & Environmental Science 5 (10) (2012) 8799–8814.

[17] P. Granger, F. Dhainaut, S. Pietrzik, P. Malfoy, A.-S. Mamede, L. Leclercq, G. Leclercq, An overview: Comparative kinetic behaviour of Pt, Rh and Pd in the NO + CO and NO + H_2 reactions, Topics in Catalysis 39 (2006) 65–76.

[18] C. N. Costa, A. M. Efstathiou, Mechanistic aspects of the H_2-SCR of NO on a novel Pt/MgO-CeO_2 catalyst, The Journal of Physical Chemistry C 111 (7) (2007) 3010–3020.

[19] C. M. Pittelkow, M. A. Adviento-Borbe, J. E. Hill, J. Six, C. van Kessel, B. A. Linquist, Yield-scaled global warming potential of annual nitrous oxide and methane emissions from continuously flooded rice in response to nitrogen input, Agriculture, Ecosystems & Environment 177 (2013) 10–20.

[20] J. Shibata, M. Hashimoto, K.-i. Shimizu, H. Yoshida, T. Hattori, A. Satsuma, Factors controlling activity and selectivity for SCR of NO by hydrogen over supported platinum catalysts, The Journal of Physical Chemistry B 108 (47) (2004) 18327–18335.

[21] I. Mejía-Centeno, S. Castillo, G. A. Fuentes, Enhanced emissions of NH_3, N_2O and H_2 from a Pd-only TWC and supported Pd model catalysts: Light-off and sulfur level studies, Applied Catalysis B: Environmental 119 (2012) 234–240.

[22] B. Torkashvand, L. Maier, M. Hettel, T. Schedlbauer, J.-D. Grunwaldt, O. Deutschmann, On the challenges and constrains of ultra-low emission limits: Formaldehyde oxidation in catalytic sinusoidal-shaped channels, Chemical Engineering Science 195 (2019) 841–850.

[23] W. P. Partridge, J. M. Storey, S. A. Lewis, R. W. Smithwick, G. L. DeVault, M. J. Cunningham, N. W. Currier, T. M. Yonushonis, Time-resolved measurements of emission transients by mass spectrometry, SAE transactions (2000) 2983–2991.

[24] D. Livio, C. Diehm, A. Donazzi, A. Beretta, O. Deutschmann, Catalytic partial oxidation of ethanol over Rh/Al_2O_3: Spatially resolved temperature and concentration profiles, Applied Catalysis A: General 467 (2013) 530–541.

[25] J. Mantzaras, Progress in non-intrusive laser-based measurements of gas-phase thermoscalars and supporting modeling near catalytic interfaces, Progress in Energy and Combustion Science 70 (2019) 169–211.

[26] R. Sui, J. Mantzaras, R. Bombach, A comparative experimental and numerical investigation of the heterogeneous and homogeneous combustion characteristics of fuel-rich methane mixtures over rhodium and platinum, Proceedings of the Combustion Institute 36 (3) (2017) 4313–4320.

[27] J. Mantzaras, R. Sui, C. K. Law, R. Bombach, Heterogeneous and homogeneous combustion of fuel-lean C_3H_8/O_2/N_2 mixtures over rhodium at pressures up to 6 bar, Proceedings of the Combustion Institute 38 (4) (2021) 6473–6482.

[28] J. Zetterberg, S. Blomberg, J. Gustafson, J. Evertsson, J. Zhou, E. C. Adams, P.-A. Carlsson, M. Aldén, E. Lundgren, Spatially and temporally resolved gas distributions around heterogeneous catalysts using infrared planar laser-induced fluorescence, Nature communications 6 (1) (2015) 7076.

[29] J. Zhou, S. Pfaff, E. Lundgren, J. Zetterberg, A convenient setup for laser-induced fluorescence imaging of both CO and CO_2 during catalytic CO oxidation, Applied Physics B 123 (2017) 1–8.

[30] J. Zhou, S. Blomberg, J. Gustafson, E. Lundgren, J. Zetterberg, Visualization of gas distribution in a model AP-XPS reactor by PLIF: CO oxidation over a Pd(100) catalyst, Catalysts 7 (1) (2017) 29.

[31] B. Zhou, E. Huang, R. Almeida, S. Gurses, A. Ungar, J. Zetterberg, A. Kulkarni, C. X. Kronawitter, D. L. Osborn, N. Hansen, et al., Near-surface imaging of the multicomponent gas phase above a silver catalyst during partial oxidation of methanol, ACS Catalysis 11 (1) (2020) 155–168.

[32] A. Zellner, R. Suntz, O. Deutschmann, Two-dimensional spatial resolution of concentration profiles in catalytic reactors by planar laser-induced fluorescence: NO reduction over diesel oxidation catalysts, Angewandte Chemie International Edition 54 (9) (2015) 2653–2655.

[33] S. Wan, B. Torkashvand, T. Häber, R. Suntz, O. Deutschmann, Investigation of HCHO catalytic oxidation over platinum using planar laser-induced fluorescence, Applied Catalysis B: Environmental 264 (2020) 118473.

[34] S. Wan, Y. Guo, T. Häber, R. Suntz, O. Deutschmann, Spatially and temporally resolved measurements of NO adsorption/desorption over NOx-storage catalyst, ChemPhysChem 21 (23) (2020) 2497–2501.

[35] S. Wan, K. Keller, P. Lott, A. B. Shirsath, S. Tischer, T. Häber, R. Suntz, O. Deutschmann, Experimental and numerical investigation of NO oxidation on Pt/Al_2O_3-and NOx storage on $Pt/BaO/Al_2O_3$-catalysts, Catalysis Science & Technology 12 (14) (2022) 4456–4470.

[36] K. Keller, S. Wan, M. Borchers, P. Lott, R. Suntz, O. Deutschmann, Treating NOx emission of hydrogen fueled combustion engines by NOx storage and reduction catalysts: A transient kinetic study including PLIF measurements, Proceedings of the Combustion Institute 39 (4) (2023) 4247–4256.

[37] A. Erdőhelyi, M. Pásztor, F. Solymosi, Catalytic hydrogenation of CO_2 over supported palladium, Journal of Catalysis 98 (1) (1986) 166–177.

[38] P. Paul, J. Gray, J. Durant Jr, J. Thoman Jr, Collisional quenching corrections for laser-induced fluorescence measurements of NO $A^2\Sigma^+$, AIAA journal 32 (8) (1994) 1670–1675.

[39] P. Paul, J. Gray, J. Durant, J. Thoman, A model for temperature-dependent collisional quenching of NO $A^2\Sigma^+$, Applied Physics B 57 (1993) 249–259.

[40] P. Paul, C. Carter, J. Gray, J. Durant Jr, J. Thoman, M. Furlanetto, Correlations for the NO $A^2\Sigma^+$ electronic quenching cross-section, Tech. rep., SAND94-8237, Sandia National Labs. (1995).

[41] M. Che, J. Dutel, P. Gallezot, M. Primet, A study of the chemisorption of nitric oxide on PdY zeolite. Evidence for a room temperature oxidative dissolution of palladium crystallites, The Journal of Physical Chemistry 80 (21) (1976) 2371–2381.

[42] K. Okumura, J. Amano, N. Yasunobu, M. Niwa, X-ray absorption fine structure study of the formation of the highly dispersed PdO over ZSM-5 and the structural change of Pd induced by adsorption of NO, The Journal of Physical Chemistry B 104 (5) (2000) 1050–1057.

[43] K. Paredis, L. K. Ono, F. Behafarid, Z. Zhang, J. C. Yang, A. I. Frenkel, B. R. Cuenya, Evolution of the structure and chemical state of Pd nanoparticles during the in situ catalytic reduction of NO with H_2, Journal of the american chemical society 133 (34) (2011) 13455–13464.

[44] B. Frank, A. Renken, Kinetics and deactivation of the NO reduction by CO on Pt-supported catalysts, Chemical Engineering & Technology: Industrial Chemistry-Plant Equipment-Process Engineering-Biotechnology 22 (6) (1999) 490–494.

[45] A. Barrera, M. Viniegra, P. Bosch, V. Lara, S. Fuentes, Pd/Al_2O_3-La_2O_3 catalysts prepared by sol-gel: characterization and catalytic activity in the NO reduction by H_2, Applied Catalysis B: Environmental 34 (2) (2001) 97–111.

[46] A. Baylet, P. Marecot, D. Duprez, P. Castellazzi, G. Groppi, P. Forzatti, In situ Raman and in situ XRD analysis of PdO reduction and Pd° oxidation supported on γ-Al_2O_3 catalyst under different atmospheres, Physical Chemistry Chemical Physics 13 (10) (2011) 4607–4613.

[47] J. Mantzaras, C. Appel, Effects of finite rate heterogeneous kinetics on homogeneous ignition in catalytically stabilized channel flow combustion, Combustion and Flame 130 (4) (2002) 336–351.

Highlights:

- 2D NO distribution is visualized via PLIF during NO reduction by H_2 over Pd/Al_2O_3.
- Adding 1% H_2O reduces the error from non-uniform quenching effect to < 3.2%.
- 2D NO distributions reveal three limiting regimes for overall NO conversion.
- The three regimes are: kinetic control, H_2 constraint and NO diffusion limitation.
- 2D data is crucial for analyzing kinetics and mass transfer interaction.

Declaration of interests

☒ The authors declare that they have no known competing financial interests or personal relationships that could have appeared to influence the work reported in this paper.

☐The authors declare the following financial interests/personal relationships which may be considered as potential competing interests: